Tellus (1995), 47B, 191–205
Printed in Belgium – all rights reserved

TELLUS
ISSN 0280–6509

Responses in NPP and carbon stores of the northern biomes to a CO_2-induced climatic change, as evaluated by the Frankfurt biosphere model (FBM)

By M. K. B. LÜDEKE*, S. DÖNGES, R. D. OTTO, J. KINDERMANN, F.-W. BADECK, P. RAMGE, U. JÄKEL and G. H. KOHLMAIER, *Institut für Physikalische und Theoretische Chemie, J. W. Goethe-Universität, Marie-Curie-Straße 11, 60439 Frankfurt am Main, Germany*

(Manuscript received 17 November 1993; in final form 2 September 1994)

ABSTRACT

To assess the role of the boreal and temperate forests and the tundra ecosystems in a future CO_2-induced climate change, the Frankfurt biosphere model (FBM) was applied to the $3 \times CO_2$ climate as calculated by the GCM of the MPI für Meteorologie in Hamburg. The FBM predicts on a $1° \times 1°$ spatial grid the seasonal and perannual course of leaf biomass and feeder roots, woody biomass, soil carbon and soil water in response to the seasonal course of light, precipitation and temperature. The phenology is controlled by the flux balance of carbon gains and losses, thus being dependent on the driving climate and the state of vegetation. Two equilibrium runs based on the $3 \times CO_2$ climate were performed: (1) Considering the pure climate effect (with no direct CO_2 fertilization) we obtained a 22% decrease of the net primary production (NPP) due to enhanced autotrophic respiration and increased water limitation. Together with the effect on the soils this results in a 170 Gt carbon source. (2) Considering a CO_2-induced enhancement of the maximum photosynthesis the pure climate effect is more than compensated and we predict a NPP increase of 9% and a total carbon sink of 50 Gt C. This effect may even be an underestimate if one takes into consideration a shift in the optimum temperature for photosynthesis under enhanced levels of atmospheric CO_2 as proposed by Long and Drake.

1. Introduction

The atmospheric concentrations of relevant greenhouse gases like CO_2 are predicted to increase continuously during the next decades. Climate model calculations using General Circulation Models (GCM's) show that an increase in surface air temperatures as well as changes in precipitation regimes and cloudiness are to be expected due to rising greenhouse gas concentrations. The role of the terrestrial biosphere within the global carbon cycle as well as within scenarios of climate change is still poorly understood. The topics being discussed intensively with respect to ecosystem response to rising CO_2 and surface air temperatures are changes of the net primary production (NPP), total biomass and soil carbon. One has to distinguish between the so-called CO_2-fertilization effect on one hand and changes due to varying climatic conditions like surface temperatures or precipitation patterns on the other hand. The CO_2-fertilization effect is considered to be one of the short-term plant responses to increased atmospheric concentration (c_a) of carbon dioxide. In general, an increase in c_a will lead to an increase in net primary production of C_3 plants (which usually work under CO_2 limitation) by accelerating the carboxylation reaction of the ribulose-1,5-bisphosphate carboxylase/oxygenase (Rubisco). However, this is not the only effect of rising CO_2 levels. Increasing c_a is also reported to modify the response of photosynthetic processes to a range of environmental variables such as tem-

* Corresponding author.

perature (Strain, 1985; Long and Hutchin, 1991), leading for instance to an increase of the temperature optimum for light-saturated photosynthesis. Consequently rising CO_2 and correlated increases in mean global temperatures will have interactive effects on plant production (Long and Drake, 1992).

In this paper, we present results of the Frankfurt Biosphere Model (FBM) concerning the response of the ecosystems of the temperate and boreal forests and polar zones of the northern hemisphere to changing environmental conditions. The Frankfurt Biosphere Model is a mechanistic and prognostic model which works in a $1.0° \times 1.0°$ lat/lon spatial resolution on a seasonal basis in which the carbon dioxide exchange between atmosphere, terrestrial biosphere and humus is computed from the corresponding daily climatic parameters of temperature, precipitation, evapotranspiration, irradiation and daylength. Using a global vegetation map and a long term average climate data base we are able to calculate the seasonal course (monthly or daily) of the state variables of biomass and humus as well as the carbon flux between the different compartments on a global scale.

In order to study the response of the ecosystems mentioned above to a CO_2-induced climate change we compare model runs driven by a "$1 \times CO_2$" climate with results gained from runs with a "$3 \times CO_2$" climate. This climate map was constructed using results from GCM-calculations performed by the Deutsches Klimarechenzentrum at the Max-Planck-Institut für Meteorologie in Hamburg which were done under the assumption of the "business-as-usual-scenario". This scenario leads to a threefold atmospheric CO_2 concentration within a time span of hundred years. From these scenario runs and the results of control runs under normal conditions we calculated regional climate anomalies which were then added to the contemporary climate.

The principal aim of our investigations presented in this paper was to study the behaviour of the temperate, boreal and tundra ecosystems under environmental conditions, which represent a "$3 \times CO_2$" climate. As described later in greater detail, we performed four model runs: one using the "$1 \times CO_2$" climate, representing the actual climatic situation, and three runs using the "$3 \times CO_2$" climate. From the latter ones the first was performed without any fertilization and the second considering CO_2 fertilization only. The third one was done with a combination of CO_2 fertilization and a shift of the GPP (gross primary production) temperature dependence towards higher temperatures.

2. The Frankfurt biosphere model

In the Frankfurt biosphere model (FBM) the vegetation is subdivided into two carbon compartments: a GC-compartment representing leaves, feeder roots and storage assimilates with a short turnover time, and a RC-compartment representing woody structural material with a longer turnover time. Gross photosynthesis (C_{ASS}) is computed daily and allocated to the two compartments from which carbon is lost by litterfall (C_{GS} and C_{RS}) and temperature dependent autotrophic respiration (C_{GA} and C_{RA}). In the current version soil organic carbon and litter are combined to one pool (SC). The calculation of heterotrophic respiration (C_{SA}) with respect to its temperature dependence is based on Fung et al. (1987). Their model was extended for consideration of available soil carbon and soil moisture. Soil water (SW) is calculated from a simple bucket model with rainfall as input and actual evapotranspiration as output. A flow chart of the model is given in Fig. 1.

In the FBM, each grid element is characterized by a vegetation type, a soil type, and the regional climate. The vegetation types are distinguished by a set of fixed parameters and a set of free parameters which are obtained through calibration.

For each vegetation type Matthews (1983, 1984) and Fung et al. (1987) give average values of maximum net primary productivity (NPP [kg C m^{-2} a^{-1}]) and biomass [kg C m^{-2}]. As there is a considerable variation of these values even within a given vegetation type it is necessary to distinguish between a characteristic climate of a vegetation type which reproduces the mean values characteristic for the entire biome and the individual climate at each location which contributes to the observed variations. The characteristic climate was obtained by an averaging process over all grid elements of a vegetation type which conserves the seasonality of the climate variables temperature, precipitation and irradiation. In

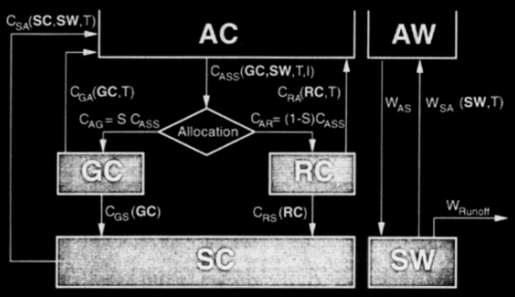

Fig. 1. Flow chart and model structure. Bold capital letters represent the reservoirs of carbon (second letter C) and water (second letter W): AC, atmospheric carbon; GC, carbon content of green biomass and feeder root biomass plus assimilate store; RC, carbon content of remaining biomass of biota; SC, carbon content of litter, humus and dead biomass; AW, water in the atmosphere; SW, soil water in the rooting zone. The capital letters C and W represent carbon and water fluxes. The indices indicate sources and sinks of these fluxes. The functional dependence of the fluxes on the driving variables and pool sizes is given in parentheses (T: hourly air temperature, I: hourly photosynthetic active radiation (PAR)). W_{AS} is the daily precipitation, W_{SA} is daily actual evapotranspiration. The factor S represents the fraction of total assimilation C_{ASS} that is allocated to GC.

practice, this was achieved by 3 steps: (1) determination of the mean months showing the maxima of the variable concerned; (2) shifting the maxima of all time series of a vegetation type to these months; (3) averaging of these superimposed time series.

The set of free parameters in the flux equations is found for each vegetation type by calibration in such a way that the model reproduces average annual NPP, annual respiration and maximum biomass when its characteristic climate is used.

The model is described in full detail by Lüdeke et al. (1994), Kindermann et al. (1993) and Janecek et al. (1989). Its verification may be summarized as follows.

The mean leaf area index of the boreal forests calculated by the Frankfurt Biosphere Model amounts to a value of 9.26 (standard deviation 2.12). 98.8 % of the grid elements of these vegetation types have LAI values ranging from 7.5 to 12.5 (Lüdeke et al., 1994). Estimations for LAI collected by Schulze (1982) are within a range of 7.4 to 9.4 for evergreen temperate forests and 7.0 to 19.0 for boreal forests. Furthermore, simulation of the LAI of cold deciduous forests results in a mean value of 4.54 (standard deviation 1.23 with 98.8 % ranging from 2.0 to 7.0). For the same vegetation type Schulze presented values between 2.4 and 7.9.

In the same paper (Lüdeke et al., 1994) we compared measured productivities along climatic gradients with the model output. We could show that an increase of NPP exists with rising latitude from 42° N to 49° N at the longitudes 142–144° W (northwest of the US) both in our model results as well as in the measured data reported by Webb et al. (1983) and Vogt et al. (1982). The annual sum of precipitation also increases in the same direction within this south–north transsect, giving clear evidence for a strong dependence of NPP on precipitation.

In the paper, mentioned above we additionally compared the biomasses calculated for the boreal forest (type 8) with the biomass inventory data for Canada (Kurz et al., 1992). Highest biomasses are found at the pacific coast, whereas the biomass decreases from the Cordilleran in the west to the central part of Canada. Here the lowest biomasses are detected. In the eastern part of Canada and at the atlantic coast the biomass of the forests increases again. This is qualitatively well reproduced by the model.

Comparing model results concerning seasonality with observations of phenology from a group of phenological gardens at different locations published by Schnelle (1985) as well as with phenological data for eastern North America reported by Schwartz and Marotz (1986) it could be shown that the flux balance criterion for phase switching used in the FBM provides a reasonable reproduction of the observed phenophases (Lüdeke et al., 1994). Leaf shooting days reported e.g., for 90° W/38° N and 84° W/43° N range from 75–80 (days after 1 January) and 110–120, respectively. The leaf shooting dates calculated by the FBM for the same locations are 78 and 111, respectively.

In addition to the thorough verification of the simulated carbon uptake and release by living biomass we also compare the model result of soil carbon to the database of Zinke et al. (1986). Their values are based on local measurements and are given as average values per Holdridge lifezone (Holdridge, 1947). As a comprehensive verification of the FBM we show in Fig. 2 the soil carbon fraction per 1°-latitudinal belt summed over all grid elements considered in this study, as

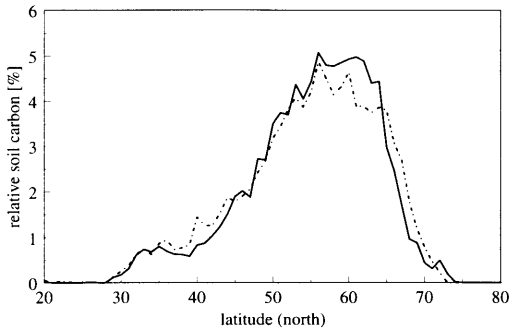

Fig. 2. Fraction of soil carbon per 1°-latitudinal belt of temperate and boreal forests as well as tundra. Solid line: simulated by the FBM, dashed line: data from Zinke et al. (1986).

a percentage of the total carbon of all those grid elements. Although the FBM predicts a total soil carbon of 32 Gt C, which is about 30% less than the data of Zinke et al. (1986), we emphasize the very good agreement in the latitudinal trend which closely resembles the climate gradient. This result underlines the ability of the model to predict possible effects and trends of a climate change on soil carbon storage.

In Fig. 5a the NPP distribution for North America as calculated by the FBM based on the present climate is displayed. Closer examination of the regions covered by boreal needle leaved forests (vegetation type 8) and mixed deciduous forests (vegetation type 10) in eastern Canada and USA reveals that the southern needle leaved forests show slightly higher NPP values than the adjacent mixed deciduous forests. At the borderline between these vegetation types (about 47°N) a NPP difference of on the average 0.08 kg m^{-2} occurs. This result which cannot be justified with respect to the existing NPP field measurements in this region reflects the uncertainty of NPP target values used in the calibration procedure. According to Fung et al. (1987) we used 0.540 kg m^{-2} for the mixed deciduous forests and the greater value of 0.585 kg m^{-2} for the boreal needle leaved forests. This difference in mean NPP values used for model calibration together with the fact that in the region under consideration the conditions for vegetation type 8 are rather favourable compared with its averaged climate while the opposite applies to type 10, explains the observed result. This shows that a revision of the NPP target values taken from the literature is to be performed, in particular with respect to the estimate for the boreal needle leaved forests, which currently is a matter of intensive debate (Wisniewski and Sampson, 1993).

2.1. *Model enlargement*

Gross carbon uptake, C_{ASS}, is modelled with a factorial approach (eq. (1)), mutiplying a maximum assimilation rate, α [g C s^{-1} m^{-2}], by 4 climate and state dependent factors (see Appendix A for details).

$$C_{ASS} = \alpha \, \mathrm{LAI(GC)} \, h_1(I, \mathrm{LAI(GC)}) \times h_2(T) \, h_3(\mathrm{SW}), \quad (1)$$

where LAI is the leaf area index [m^2 m^{-2}], I is the radiation flux density [W m^{-2}], and T is the temperature [°C]. The maximum assimilation rate as well as the free parameters in the respiration flux equations are determined by calibration.

The response of α to an increased atmospheric CO_2 concentration can be simulated by the following function (Kirschbaum and Farquhar, 1987; McMurtrie et al., 1993)

$$f(\mathrm{CO_2}, T) = \frac{c_i - \Gamma^*(T)}{c_i + 2\,\Gamma^*(T)}, \quad (2)$$

where the internal CO_2 concentration in the leaves of C_3 plants is estimated to be 70% of the external concentration (Wong et al., 1979) and the CO_2 compensation point (for gross photosynthesis and photorespiration), $\Gamma^*(T)$ [ppmv], at any temperature is given by (Kirschbaum, 1993)

$$\Gamma^* = 40.6 \, e^{\{9.46(T-25)/(T+273.2)\}}. \quad (3)$$

In the FBM, the change in maximum productivity with changing CO_2 concentration and temperature is then simulated as

$$\alpha(\mathrm{CO_2}, T) = \alpha_0(\mathrm{CO_2^0}, T^0) \times \frac{f(\mathrm{CO_2}, T)}{f(\mathrm{CO_2^0}, T^0)}, \quad (4)$$

where CO_2^0 and T^0 are the current CO_2 content (350 ppmv) and temperature, respectively. For the calculation of the new maximum assimilation rate with eq. (4) we did not consider the seasonal variation of temperature as it is done with the flux equa-

Table 1. *Vegetation types used for this study*

id #	Name of vegetation type (biome)	Area [10^6 km^2]
8	temperate/subpolar evergreen needleleaved forest	9.5
10	cold-deciduous forest, with evergreens	7.7
11	cold-deciduous forest, without evergreens	5.5
14	evergreen needleleaved woodland	2.3
16	cold-deciduous woodland (larch forest)	2.7
18	evergreen needleleaved/microphyllous shrubland/thicket	0.4
20	cold-deciduous subalpine/subpolar shrubland, dwarf shrubland	0.5
22	arctic/alpine tundra, mossy bog	7.6
	total area	36.2

tions but rather the average daylight temperature ($T_{\varnothing}$) during the vegetation period in the characteristic climate of each vegetation type.

The second effect of an increase in atmospheric CO_2 concentration is an increase in the optimum temperature of light saturated photosynthesis as proposed by Long and Drake (1992). This has been observed in some measurements on C_3 leaves (Berry and Björkman, 1980; Osmond et al., 1980; Pearcy and Björkman, 1983). To test this possible effect on the biospheric behaviour in a $3 \times CO_2$-climate with our model we shifted optimum and maximum temperature of gross photosynthesis by 10°C which is a value suggested by Long and Drake (1992) from their more mechanistic studies of a possible fertilization effect (see Appendix C).

2.2. *Data bases*

The vegetation distribution as used in the FBM is based on Matthews (1983, 1984), whose classification is based on physiognomy rather than being correlated directly with climate. All together now, 32 vegetation types are distinguished out of which 8 types were selected to study the impact of a change in climate on temperate and boreal forests as well as tundra ecosystems (Table 1).

Each soil type is assigned a field capacity and a permanent wilting point (Dönges, 1992), soil organic carbon is taken from the data reported by Atjay et al. (1979), Post et al. (1985), and Schlesinger (1984).

To simulate the equilibrium, carbon exchange fluxes under the present-day climate regime we used the long-term average climate data base from Shea (1986). It contains monthly average data of temperature and precipitation on a 2.5° by 2.5° grid which we interpolated to daily values on a 1° by 1° grid.

The changes from the present climate to a greenhouse climate under an effective concentration of $3 \times CO_2$ is taken from the results of a transient General Circulation Model run (business as usual) performed by the Max Planck Institute für Meteorologie in Hamburg (Claussen, 1993; Perlwitz, 1992). Starting in 1985 the GCM was run with a coupled ocean model for 100 years until the atmospheric CO_2 concentration approached 1050 ppmv. From there on the simulation proceeded with a constant seasonal ocean cycle and constant CO_2 concentration for another 30 years. We interprete the average of these 30 years as the equilibrium climate. The difference between this future climate and a control simulation of the contemporary climate, done with the same GCM, was added to the long-term average values from Shea (1986) and interpolated to the model resolution to determine the input data for the future climate scenario.

In Fig. 3 we show a diagram of the characteristic climate of the temperate evergreen needle-leaved forests. In this diagram we compare the present temperature and precipitation courses with the values simulated for the $3 \times CO_2$ climate. We recognize an increase in temperature of more than three degrees in summer and more than five degrees in winter and an increase in precipitation between 10 and 20%. A similar behaviour is observed for the other vegetation types with an additional phase shift of temperature or precipitation of about one month for the types 10, 11, 16 and 20.

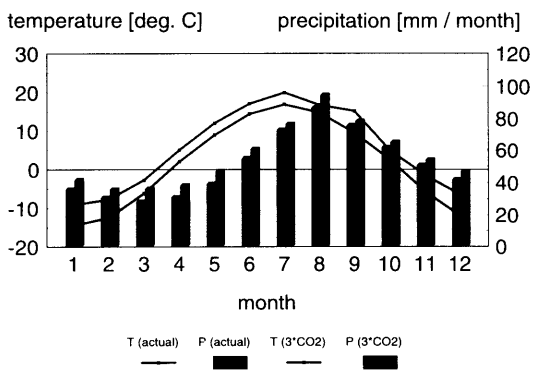

Fig. 3. Average climate of temperate/subpolar evergreen needleleaved forest using actual and $3 \times CO_2$ climate data.

A detailed comparison of the changes in summer temperature for all grid elements considered in this study reveals a mean increase of about 3°, whereas 4° and 5° increases are observed in the eastern United States and in Siberia.

3. Simulation runs

To assess the future behaviour of temperate and boreal forests and the tundra ecosystems, 3 equilibrium model runs were performed.

(I) A reference run using the actual climate represented by the Shea Climate Atlas (1986).

(II) A model run using the $3 \times CO_2$ climate (see previous section) neglecting a CO_2-fertilization effect.

(III) A model run using the $3 \times CO_2$ climate including the CO_2-fertilization effect with respect to stimulation of photosynthesis.

Comparison of the results of runs I and II will allow for estimation of the pure climate effect on vegetation in a $3 \times CO_2$ environment. The prognosticated changes in temperature and precipitation will influence photosynthesis as well as autotrophic and heterotrophic respiration. To identify the causes of the changes in net primary production and the state of vegetation in the $3 \times CO_2$ climate further model runs for the vegetation types 8 and 11 were performed. To separate the effect of changes in the water budget on photosynthesis from the pure temperature effect on photosynthesis and autotrophic respiration we performed a $3 \times CO_2$ run using the daily water limitation factors (h_3, see eq. (1)) from the reference run ($1 \times CO_2$).

In run III, a pure stimulation of photosynthesis, represented by an enhanced maximum photosynthetic rate α is assumed, allowing for a comparison with the corresponding results calculated with the "Terrestrial Ecosystem Model (TEM)" (Melillo et al., 1993). As described in Section 2, the increase of α is determined by the vegetation type dependent average daylight temperature during the vegetation period and the increase of atmospheric CO_2 concentration from 350 ppm ($1 \times CO_2$) to 1050 ppm ($3 \times CO_2$). The temperature values are displayed in Table 2 whereas the corresponding α-values used for the different model runs (determined using eq. (4)) are shown in Table 3. The remaining vegetation type specific parameters which do not change with the different model runs are given in Appendix B.

The numerical procedure to find the equilibrium of vegetation and soil at each grid element uses a modified bracketing and bisectioning method. Starting with the calibration values of the state variables a one year cycle is calculated. According to the sign of the difference of net primary production and annual litter production the starting values for the next one year run are modified. This procedure is repeated until the difference becomes smaller than a given tolerance value indicating that the equilibrium limit cycle is reached. The evaluation of the model equations yields in the case of deciduous vegetation for a few grid

Table 2. *Average daylight temperature ($T_\varnothing$) during the vegetation period in the characteristic climate of the corresponding vegetation type*

Vegetation type	8	10	11	14	16	18	20	22
$T_\varnothing$, $1 \times CO_2$ [°C]	10.3	12.6	11.9	8.2	9.5	8.4	7.5	7.0
$T_\varnothing$, $3 \times CO_2$ [°C]	12.1	14.2	14.1	11.4	12.5	11.4	9.2	8.5

Table 3. *Parameters used in the different runs for the vegetation types 8, 10, 11, 14, 16, 18, 20 and 22 (first column); second column: Run I: 1 × CO_2-climate equilibrium run. Run II: 3 × CO_2-climate equilibrium run without fertilization. Run III: 3 × CO_2-climate equilibrium run with fertilization effect, assuming a rise of maximum photosynthesis rate α*

VT	Run	α [kg m^{-2} s^{-1}]
8	(I), (II)	$2.8436 \cdot 10^{-8}$
	(III)	$3.4410 \cdot 10^{-8}$
10	(I), (II)	$4.4096 \cdot 10^{-8}$
	(III)	$5.4240 \cdot 10^{-8}$
11	(I), (II)	$5.8942 \cdot 10^{-8}$
	(III)	$7.1910 \cdot 10^{-8}$
14	(I), (II)	$1.6882 \cdot 10^{-8}$
	(III)	$2.0090 \cdot 10^{-8}$
16	(I), (II)	$1.0500 \cdot 10^{-8}$
	(III)	$1.2600 \cdot 10^{-8}$
18	(I), (II)	$1.5873 \cdot 10^{-8}$
	(III)	$1.8890 \cdot 10^{-8}$
20	(I), (II)	$4.6166 \cdot 10^{-8}$
	(III)	$5.4940 \cdot 10^{-8}$
22	(I), (II)	$2.8113 \cdot 10^{-8}$
	(III)	$3.3450 \cdot 10^{-8}$

elements (0–10%, depending on vegetation type) a stable limit cycle with a period of n years, $n > 1$. A closer examination shows that this phenomenon appears only in the case of grid elements with climatic conditions far away from the typical climate. This is partly caused by inconsistencies concerning the vegetation map and the more coarsely gridded climate atlas. To solve this problem of nonbiological behaviour we deviated in these cases from the principle of constant parameter values for an entire vegetation type, allowing for acclimation of the temperature response of photosynthesis and autotrophic respiration. It occurs that a simultaneous shift of both response functions which is in accordance with observational results (Berry and Raison, 1981) leads to stable one-year limit cycles.

4. Results and discussion

Table 4 gives an overview of total net primary production (NPP) and total carbon content (TCC) of the vegetation types investigated within three different simulation runs. In Figs. 5 and 7 the regional NPP distributions for North America (this is about 1/3 of the grid elements considered) are displayed.

(a) Run II versus run I

As a first interesting result, the NPP tends to decrease when only the climatic effects of the 3 × CO_2 environment are considered (I versus II, Table 4). The total NPP of the vegetation types investigated in simulation II decreases by 22%, the total carbon storage by 27.7% corresponding to a net carbon source of 170 Gt C over 100 years. Comparison of the regional NPP distributions shows that most of the vegetation types contribute to this decrease; a small increase in the tundra

Table 4. *Resulting net primary production (NPP) and total carbon content (TCC) for the vegetation types investigated within the 3 different simulation runs*

VT	I: NPP [Gt a^{-1}]	II: NPP [Gt a^{-1}]	III: NPP [Gt a^{-1}]	I: TCC [Gt]	II: TCC [Gt]	III: TCC [Gt]
8	5.364	4.502	5.556	243.49	185.50	239.16
10	3.248	2.011	3.356	141.12	84.120	145.39
11	2.756	2.008	2.937	114.54	77.553	117.65
14	0.343	0.320	0.489	15.333	13.027	21.481
16	0.682	0.657	0.959	23.600	21.320	31.603
18	0.113	0.099	0.148	4.340	3.380	5.100
20	0.113	0.114	0.176	1.915	1.886	3.119
22	0.580	0.586	0.922	68.912	56.428	100.06
Σ	13.199	10.297	14.543	613.25	443.21	663.56

Tellus B/47/1/2-15

Table 5. *Results of closer examination of the temperature effect on GPP and Respiration for vegetation type 8 in North America after changing the 1 × CO_2-climate into the 3 × CO_2-climate*

	Simulation run I 1 × CO_2 climate	Simulation run IIa 1 × CO_2 water budget and 3 × CO_2 temperature	Simulation run II 3 × CO_2 climate
GPP (mean value) [kg m^{-2} a^{-1}]	1.200	1.242 increase +3.5% ≅ 42 g	1.156 decrease −3.6% ≅ 44 g
RES (mean value) [kg m^{-2} a^{-1}]	0.641	0.738 increase +15.13% ≅ 97 g	0.677 increase +5.62% ≅ 36 g
GPP − RES = NPP (mean value) [kg m^{-2} a^{-1}]	0.559	0.504	0.479

ecosystem (Figs. 5a and 7) is overcompensated by the NPP losses, mainly in the south east.

Two possible causes for this decrease are on the one hand the direct temperature effect increasing autotrophic respiration more than photosynthesis and on the other hand changes in the water balance (Lüdeke et al., 1994).

In order to distinguish between the effects of temperature and water stress we performed an additional type II simulation (IIa) for vegetation types 8 and 11 where only the 3 × CO_2 temperature is implemented while the water regime is left unchanged. The results in Table 6 indicate that the direct effect of temperature is the main cause for NPP reduction in type 8 (which is a typical result for most of the vegetation types investigated here) while for type 11 the effects of temperature and water limitation are of similar significance. A closer examination of the pure temperature effect reveals that the NPP reduction is mainly caused by an increase in autotrophic respiration. As expected, vegetation type 8 in Northern America shows an increase in autotrophic respiration by +15% (Table 5) while GPP increases by +3.5%. This is due to the suboptimal photosynthetic production with respect to the "ambient CO_2" temperature.

Subsequently we want to examine the effects of changes in the water balance in more detail:

When the effect of water limitation is taken into consideration (run II) both GPP and respiration decrease compared to the pure temperature simulation IIa (Table 5). As soil water availability is reduced (see Fig. 4) in the 3 × CO_2 climate, higher water stress, expressed by the factor h_3(SW), causes a reduction of GPP. Fig. 4 shows for all grid elements of vegetation types 8 and 11 how the annual minima of the water factor h_3(SW) are shifted towards lower values, representing the strongest water stress which the plants are exposed to within a year. The average minimum of the water factor decreases by 10% for vegetation type 8 and by 14% for vegetation type 11, limiting photosynthesis very strongly. As already men-

Table 6. *Results of examination of water budget and temperature contribution to NPP reduction after changing the 1 × CO_2-climate into the 3 × CO_2-climate*

VT	Run I NPP [Gt a^{-1}]	Run IIa NPP [Gt a^{-1}]	Run II NPP [Gt a^{-1}]	Rel. contribution to reduction temperature	water budget
8	5.364	4.804	4.502	65%	35%
11	2.756	2.416	2.008	45.5%	54.5%

Run I is the reference run driven by the 1 × CO_2-climate. For run II, the 3 × CO_2 climate is used. Run IIa was performed with the 3 × CO_2-climate but with the water budget of run I.

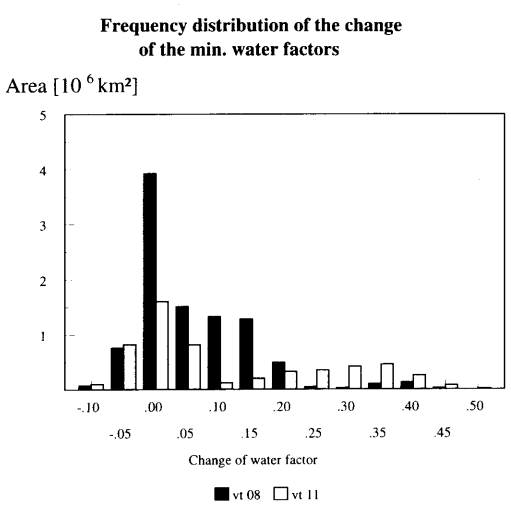

Fig. 4. Frequency distribution of the absolute change in the minimum water factor which occurs when the $3 \times CO_2$ climate is compared with the $1 \times CO_2$ climate. The positive sign of the difference indicates that there is an increase of water limitation in the $3 \times CO_2$ climate.

tioned in Section 2, there was a detailed validation of the model referring to its ability to reproduce observed NPP water limitations.

As a consequence of lower GPP, the standing biomass decreases too, causing a reduction of autotrophic respiration. This is the reason why respiration responds to water stress although it is not directly depending on water availability.

The overall effect of temperature and water balance is shown in Table 5 for vegetation type 8: GPP decreases in the $3 \times CO_2$ climate (-3.6%) but respiration increases ($+5.6\%$). From these results we conclude that the general decrease of NPP in the $3 \times CO_2$ climate is caused by (1) higher respiration due to higher temperature and (2) lower photosynthesis due to water limitation.

With respect to the temperature response it should be mentioned that the rather simple exponential approach for estimating autotrophic respiration may cause an overestimation of the temperature response, although the Q_{10} values we use are within the range cited in the literature (Ryan, 1991, for a list). In this context it should be mentioned that there are indications for a more linear increase in respiration with temperature when long term effects (hours to days) are studied compared to exponential response functions resulting from experiments with rather fast temperature changes (Semichatova, 1974). As Ryan (1991) states, the use of functional models that distinguish between maintenance and growth respiration predict a lower response to increased temperature. A possible acclimation of respiration to changing temperature is not yet well understood and therefore difficult to quantify.

A direct quantitative comparison of the results presented above with the results of a similar study based on the Terrestrial Ecosystem Model (TEM) by Melillo et al. (1993) is not possible because different climate predictions were used. First attempts were made to test the response of the FBM to other climate scenarios showing a strong dependence of the model results on the particular GCM output, mainly due to water limitation. Furthermore direct model intercomparisons (including TEM) on the basis of common driving variables are under way.

The TEM study cited above calculates a 10% increase of NPP of the northern biomes for the pure climate effect without consideration of the CO_2-fertilization effect, while the study presented here predicts a 22% decrease. Unfortunately the TEM study does not analyze how the overall increase is particularly composed of the BPP response due to modifications in water limitation and temperature as well as of changes in autotrophic respiration and nitrogen mineralization due to temperature change. Thus even a qualitative comparison of the model behaviour with respect to common variables like BPP and autotrophic respiration is difficult. However, the TEM authors' postulation that increased NPP is due to increased nitrogen mineralization in a double CO_2 climate leads to the assumption that the consideration of nitrogen dynamics, as planned in a future FBM version, will partially compensate the negative climate effect on NPP stated in this study.

(b) Run III versus run I

If, in addition, the proposed increase in the maximum assimilation rate (α) due to higher CO_2 concentrations at all temperatures is taken into account the NPP decrease calculated in simulation II is more than compensated and we predict an increase of 9.2% in overall NPP and of 8.2% in total carbon content which corresponds to a carbon sink of 50.3 Gt during the next one hundred years. The same trend is predicted by

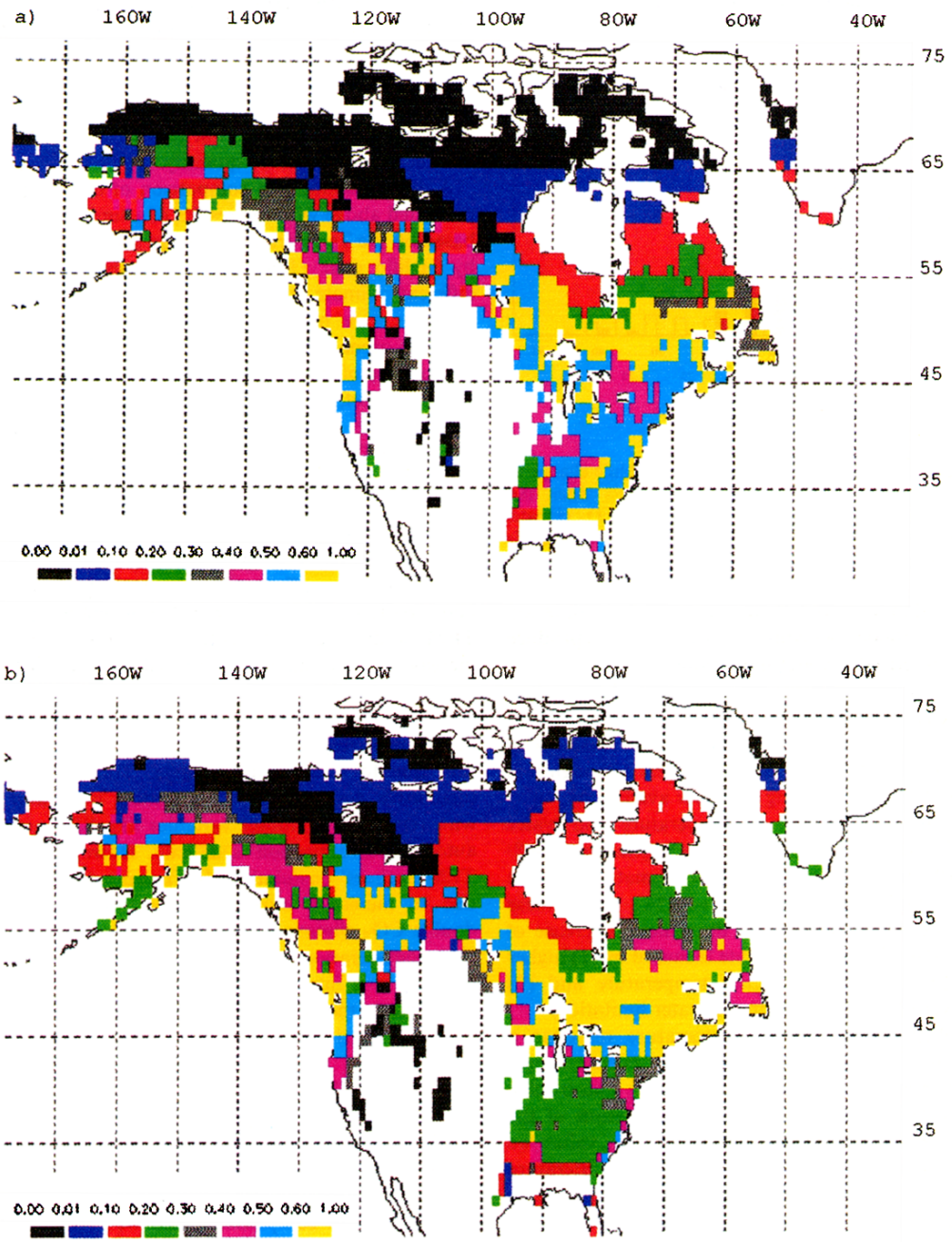

Fig. 5. (a) Regional NPP distribution of reference run I [kg m^{-2} a^{-1}]. (b) Regional NPP distribution of run III [kg m^{-2} a^{-1}]; driven by the $3 \times CO_2$-climate including a fertilization effect.

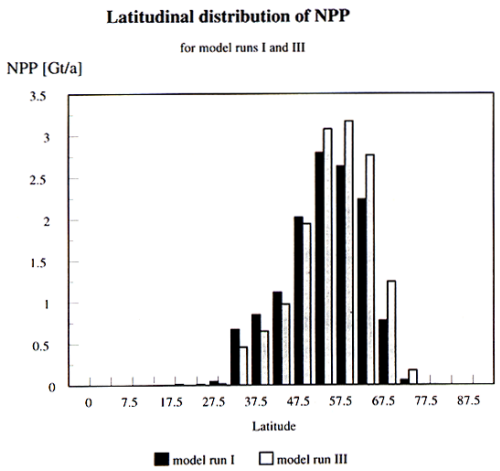

Fig. 6. NPP of latitudinal 5° belts for the $1 \times CO_2$-climate (run I) and $3 \times CO_2$-climate with fertilization effect (run III).

Melillo et al. (1993) using different double CO_2 climates.

A more detailed comparison of the runs I and III (Fig. 5) shows a NPP shift northward, produced by an increase of tundra NPP and a decrease mainly in the deciduous forest ecosystems (types 10 and 11) in the south east due to increased water limitation and autotrophic respiration. Field measurements in tundra ecosystems (Mooney et al., 1991) confirm a persistent NPP increase for a simultaneous increase in CO_2 concentration and temperature. Examination of the latitudinal distribution of the calculated NPP for the total area considered (including Eurasia, Fig. 6) shows that the northward shift of maximum NPP applies to the whole complex of temperate and boreal forests and tundra ecosystems.

It has been suggested by Long and Drake (1992) who evaluated the Farquhar photosynthesis model that the optimum temperature for primary production shifts to higher temperatures as the atmospheric CO_2 levels are increased. In a first attempt to include this effect in our model we shifted the optimum and maximum temperature for the $3 \times CO_2$ case by 10 K relative to the temperature course of run III, as shown in Appendix C. It became immediately obvious that for photosynthesis at suboptimum temperatures, the production was decreased. The reason for this is due to the choosen product function of CO_2-fertilization and the temperature function h_2. In a simulation

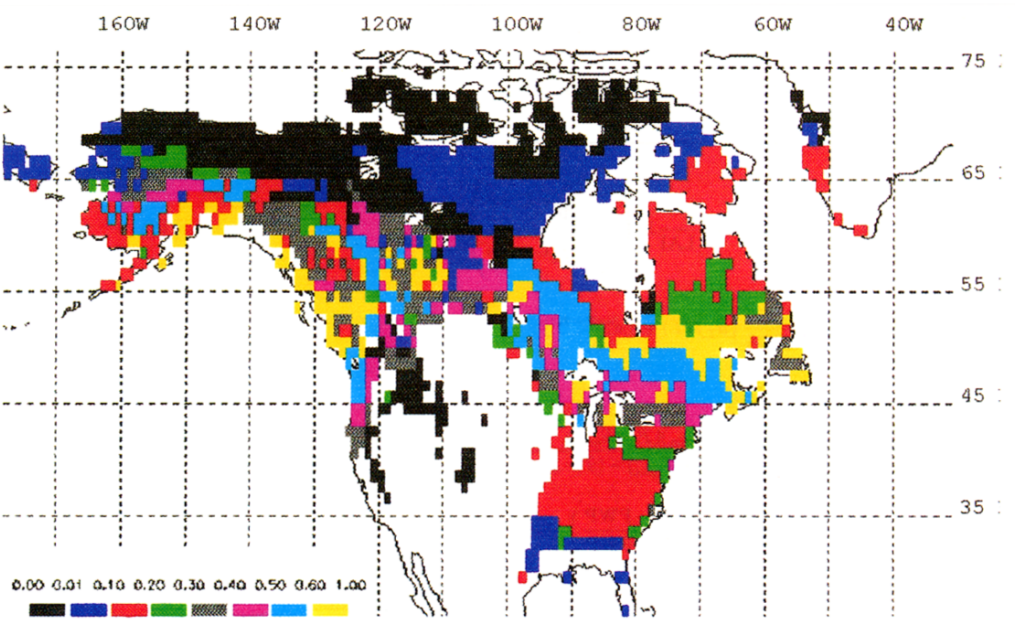

Fig. 7. Regional NPP distribution of run II [kg m^{-2} a^{-1}]; $3 \times CO_2$-climate without fertilization effect.

with the full Farquhar model, this seperation is no longer possible. In accordance with Long and Drake (1992), we have choosen a CO_2 temperature dependence wich follows qualitatively their suggested behaviour, as shown in Appendix C. It was very suprising to see that the net primary production of the boreal ecosystems was increased in such a scenario by about 30% over the reference case while the tundra showed an even stronger effect perhaps due also to the lengthening of the growing season. In summary we would like to state that the combined CO_2-temperature effect on potosynthesis has a very strong influence on the future carbon balance in these ecosystems. Unfortunately there is very little empirical information how the plant photosynthesis will react in the long range to such a combined climate and CO_2 change.

Modelling experiments discussed above demonstrate the importance of direct and indirect temperature effects as well as CO_2 fertilization on NPP. The modelization of the temperature response of autotrophic respiration, heterotrophic respiration, and water balance in the ecosystem can be identified as crucial points which deserve closer examination.

5. Acknowledgements

We thank the European Union and the German Ministry of Research and Technology for financial support. Helpful comments of Dr. Colin Prentice and an anonymous reviewer are gratefully acknowledged. We thank Gudrun Würth for many helpful discussions concerning biological questions and Christof Häger and Torsten Lang for their considerable support of the numerical evaluations.

6. Appendix

(A) Flux equations

Table 7. *Factors (between 0 and 1) used to describe gross assimilation as a function of state and climate in eq. (1)*

$$h_1(I, \mathrm{LAI(GC)}) = \frac{1}{k\,\mathrm{LAI}} \ln\left(\frac{\frac{\alpha}{\Phi} + I}{\frac{\alpha}{\Phi} + I\,\mathrm{e}^{(-k\,\mathrm{LAI})}}\right) \tag{5}$$

$$h_2(T) = \frac{2}{\alpha\,\mathrm{SLA}}\left\{a_T f(T) + \beta\,\mathrm{e}^{\omega(T-T_0)}\right\} \tag{6}$$

with

$$f(T) = \frac{(T-T_{\min})(T-T_{\max})}{(T-T_{\min})(T-T_{\max}) - (T-T_{\mathrm{opt}})^2}$$

$$h_3(\mathrm{SW}) = \frac{\tanh\left(a_{\mathrm{SW}}\frac{\mathrm{SW}-\mathrm{PWP}}{\mathrm{FC}-\mathrm{PWP}}\right)}{\tanh(a_{\mathrm{SW}})} \tag{7}$$

I: incident radiation above canopy [W m^{-2}], PWP: permanent wilting point, FC: field capacity, $a_{\mathrm{SW}} = 1.946$, for other variables see Tables 3, 8 and 9).

(B) Parameters

Table 8. *Parameter sets independent of the calibration procedure for all vegetation types considered in this study*

Parameter	Type 08	Type 10	Type 11	Type 14	Type 16	Type 18	Type 20	Type 22
Target values for the calibration procedure								
GC_{max} [kg m^{-2}]	1.6	0.252	0.25	1.08	0.33	0.16	0.38	0.23
RC_{max} [kg m^{-2}]	11.8	12.4	12.4	5.67	5.08	2.54	2.32	0.23
SC_{max} [kg m^{-2}]	14.0	12.0	12.0	9.0	8.0	10.0	6.5	19.0
NPP [kg m^{-2} a^{-1}]	0.585	0.54	0.54	0.35	0.36	0.285	0.275	0.1
ResG* [kg m^{-2} a^{-1}]	0.29	0.27	0.27	0.18	0.18	0.14	0.14	0.12
ResR* [kg m^{-2} a^{-1}]	0.29	0.27	0.27	0.18	0.18	0.14	0.14	0.12
LpG* [kg m^{-2} a^{-1}]	0.53	0.176	0.176	0.324	0.259	0.048	0.251	0.09
Temperature dependence of net photosynthesis								
T_{min} [K]	270.6	273	273	270.6	273	270.6	270.1	270.1
T_{max} [K]	311.6	313	313	311.6	313	311.6	313.1	312.1
T_{opt} [K]	290.6	294	294	290.6	294	290.6	288.1	288.1
Light absorption coefficient per leaf layer								
k [-]	0.5	0.5	0.5	0.5	0.5	0.5	0.5	0.5
Initial quantum yield								
Φ [kg J^{-1}]	$2.56 \cdot 10^{-9}$	$2.56 \cdot 10^{-9}$	$2.56 \cdot 10^{-9}$	$2.56 \cdot 10^{-9}$	$2.56 \cdot 10^{-9}$	$2.56 \cdot 10^{-9}$	$2.56 \cdot 10^{-9}$	$2.56 \cdot 10^{-9}$
Specific leaf area								
SLA [m^2 kg^{-1}]	12	40	40	12	27	12	20	30
Temperature coefficient in the argument of exponential function for autotroph respiration								
ω [K^{-1}]	0.0833	0.0833	0.0800	0.0833	0.0833	0.0833	0.041	0.41
Soil type with respect to temperature response (after Fung et al., 1987)								
RG [-]	3	2	2	3	3	3	4	2
Parameter determining the allometric relation between GC and RC								
κ [-]	1.6	1.6	1.6	1.6	1.6	1.6	1.6	1.6
ξ [(kg m^{-2})$^{1/\kappa}$]	5.49	112.04	112.04	5.01	30.81	47.67	10.91	2.447

* ResG, ResR and LpG denote the estimated mean annual values for the autotroph respiration of GC and RC and the litter production of GC, used in the calibration procedure.

Table 9. *Parameter sets determined by calibration for all vegetation types considered in this study*

	Type 8	Type 10	Type 11	Type 14	Type 16	Type 18	Type 20	Type 22
β, C_{GA}	$1.78 \cdot 10^{-8}$	$8.95 \cdot 10^{-8}$	$1.21 \cdot 10^{-7}$	$1.72 \cdot 10^{-8}$	$1.19 \cdot 10^{-7}$	$1.22 \cdot 10^{-7}$	$5.64 \cdot 10^{-8}$	$7.76 \cdot 10^{-8}$
γ, C_{RA}	$2.36 \cdot 10^{-9}$	$1.39 \cdot 10^{-9}$	$1.96 \cdot 10^{-9}$†	$3.17 \cdot 10^{-9}$	$5.37 \cdot 10^{-9}$	$7.49 \cdot 10^{-9}$	$4.77 \cdot 10^{-9}$	$4.95 \cdot 10^{-8}$
δ, C_{RS}	$1.34 \cdot 10^{-10}$	$9.40 \cdot 10^{-10}$	$9.41 \cdot 10^{-10}$	$1.46 \cdot 10^{-10}$	$6.33 \cdot 10^{-10}$	$3.03 \cdot 10^{-9}$	$3.25 \cdot 10^{-10}$	$1.19 \cdot 10^{-9}$
ε*, C_{GS}	$1.11 \cdot 10^{-8}$	—	—	$1.00 \cdot 10^{-8}$	—	$1.05 \cdot 10^{-8}$	—	—
η, C_{SA}	$1.43 \cdot 10^{-9}$	$7.29 \cdot 10^{-10}$	$1.11 \cdot 10^{-9}$	$1.14 \cdot 10^{-9}$	$2.92 \cdot 10^{-9}$	$9.09 \cdot 10^{-10}$	$9.09 \cdot 10^{-10}$	$2.98 \cdot 10^{-10}$

All fluxes (see Fig. 1) are donor controlled and the Greek letters denote the corresponding rate coefficients [s^{-1}].
* Continuous litter production rate coefficient, only for evergreen vegetation types.
† In this case, $\omega = 0.0833$.

(C) Temperature dependence of photosynthesis

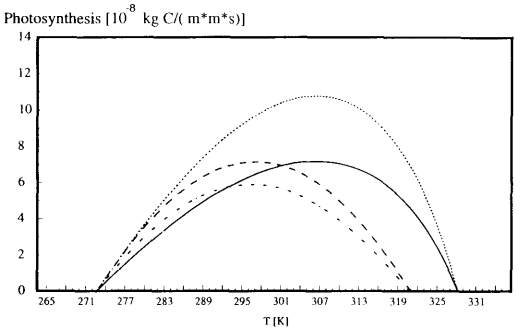

Fig. 8. Temperature dependence of photosynthesis (light saturation, maximum LAI) of vegetation type 11 (cold deciduous forests): (a) chained line: reference run, no fertilization; (b) long-dashed line: run III, CO_2-fertilization by enhancement of maximum photosynthetic rate. (c) solid line: CO_2-fertilization as in run III additionally shifting T_{opt} and T_{max}, resulting in an unrealistic behaviour at low temperatures ($273 < T < 292$); (d) short-dashed line: same as (c) but additionally fitted to the results of Long and Drake (1992).

REFERENCES

Ajtay, G. L., Ketner, P. and Duvigneaud, P. 1979. Terrestrial primary production and phytomass. In: *SCOPE* **13**, The global carbon cycle, 129–181.

Berry, J. A. and Björkman, O. 1980. Photosynthetic response and adaption to temperature in higher plants. *Ann. Rev. Plant. Physiol.* **31**, 491–543.

Berry, J. A. and Raison, J. K. 1981. Responses of macrophytes to temperature. In: *Encyclopedia of plant physiology 12A: Physiological plant ecology* (ed. Lange, Nobel, Osmond, Ziegler). Berlin: 278–338.

Claussen, M. 1993. *Shift of biome pattern due to simulated climate variability and climate change.* Report No. 115. Max Planck-Institut für Meteorologie, Hamburg, Germany.

Dönges, S. 1992. *Numerische Simulation der Evapotranspiration und des Bodenwasserhaushaltes unterschiedlicher Ökosysteme als Funktion charakteristischer Klimaparameter.* Diploma Thesis.

Fung, I. Y., Tucker, C. J. and Prentice, K. C. 1987. Application of advanced very high resolution radiometer vegetation index to study atmosphere-biosphere exchange of CO_2. *J. Geophys. Res.* **92**(D3), 2999–3015.

Holdridge, L. R. 1947. Determination of world plant formations from simple climatic data. *Science* **105**, 367–368.

Janecek, A., Benderoth, G., Lüdeke, M. K. B., Kindermann, J. and Kohlmaier, G. H. 1989. Model of the seasonal and perennial carbon dynamics in deciduous-type forests controlled by climatic variables. *Eco. Mod.* **49**, 101–124.

Kindermann, J., Lüdeke, M. K. B., Badeck, F.-W., Otto, R. D., Klaudius, A., Häger, Ch., Würth, G., Lang, T., Dönges, S., Habermehl, S. and Kohlmaier, G. H. 1993. Structure of a global carbon exchange model for the terrestrial biosphere. *Water, Air & Soil Pollution* **70**, 675–684.

Kirschbaum, M. U. F. and Farquhar, G. D. 1987. Investigation of the CO_2 dependence of quantum yield and respiration in Eucalyptus pauciflora. *Plant Physiol.* **83**, 1032–1036.

Kirschbaum, M. U. F. 1993. A modelling study of the effects of changes in atmospheric CO_2 concentration, temperature and atmospheric nitrogen input on soil organic carbon storage. *Tellus* **45B**, 321–334.

Kurz, W. A., Apps, M. J., Webb, T. M. and McNamee, P. J. 1992. *The carbon budget of the Canadian forest sector:* Phase I. Information Report NOR-X-326, Forestry Canada, Northwest Region, Northern Forestry Centre, Alberta.

Long, S. P. and Hutchin, P. R. 1991. Primary production in grasslands and coniferous forests with climate change: an overview. *Ecological Applications* **1**, 139–156.

Long, S. P. and Drake, B. G. 1992. Photosynthetic CO_2 assimilation and rising atmospheric CO_2 concentra-

tions. In: *Crop photosynthesis: spatial and temporal determinants* (ed. N. R. Baker and H. Thomas). Elsevier pp. 69–103.

Lüdeke, M. K. B., Badeck, F.-W., Otto, R. D., Häger, C., Dönges, S., Kindermann, J., Würth, G., Lang, T., Jäkel, U., Klaudius, A., Ramge, P., Habermehl, S. and Kohlmaier, G. H. 1994. The Frankfurt biosphere model. A global process oriented model for the seasonal and longterm CO_2 exchange between terrestrial ecosystems and the atmosphere. *Climate Research* **4**, 143–166.

Matthews, E. 1983. Global vegetation and land use: new high–resolution data bases for climate studies. *J. Clim. Appl. Meteor.* **22**, 474–487.

Matthews, E. 1984. Global inventury of pre-agricultural and present biomass. *Progress in Biometeorology* **3**, 237–246.

McMurtrie, R. E. 1993. Modelling of canopy carbon and water balance. In: *Photosynthesis and production in a changing environment, a field and laboratory manual* (ed. Hall, D. O., Scurlock, J. M. O., Bolhar-Nordenkampf, H. R., Leegood, R. C. and Long, S. P.). Chapman and Hall, London.

Melillo, J. M., McGuire, A. D., Kicklighter, D. W., Moore III, B., Vörösmarty, C. J. and Schloss, A. L. 1993. Global climate change and terrestrial net primary production. *Nature* **363**, 234–240.

Mooney, H. A., Drake, B. G., Luxmoore, W. C., Oechel, W. C. and Pitelka, L. F. 1991. Predicting ecosystem responses to elevated CO_2 concentrations. *BioScience* **41**, 96–104.

Osmond, C. B., Björkman, O. and Anderson, D. J. 1980. Physiological processes in plant ecology. *Ecological studies* **36**, Springer-Verlag, Berlin.

Pearcy, R. W. and Björkman, O. 1983. In: *CO_2 and plants: the response of plants to rising levels of atmospheric carbon dioxide* (ed. Lemon, E. R.). Westview Press, Boulder, CO, 65–105.

Perlwitz, J. 1992. Preliminary results of a global SST anomaly experiment with a T42 GCM. *Annales Geophysicae Assembly of the European Geophysical Society*. Edinburgh, 6–10 April 1992.

Post, W. M., Pastor, J., Zinke, P. J. and Stangenberger, A. G. 1985. Global patterns of soil nitrogen storage. *Nature* **317**, 613–616.

Schlesinger, W. H. 1984. Soil organic matter: a source of atmospheric CO_2. In: *The rôle of terrestrial vegetation in the global carbon cycle: measurement by remote sensing. SCOPE* **23** (ed. G. M. Woodwell). J. Wiley & Sons, pp. 111–127.

Schnelle, F. 1985. 10jährige Mittel (Zeiträume 1963–1972 und 1973–1982) für 17 Phasen, die in 13 IPG beobachtet wurden. *Arboreta Phaenologica* **29**, 12–28.

Schwartz, D. M. and Marotz, G. A. 1986. An approach to examing regional atmosphere-plant interactions with phenological data. *Journal of Biogeography* **13**, 551–560.

Semichatova, O. A. 1974. *Energetika dychanija rastenii pri povyšennoi temperature*. Izd. Nauka, Leningrad.

Shea, D. J. 1986. *Climatological atlas: 1950–1979*. Surface air temperature, precipitation, sea-level pressure, and sea-surface temperature (45°S–90°N). NCAR Technical Note 269 + STR. NCAR, Boulder, Colorado.

Strain, B. R. 1985. Physiological and ecological controls on carbon sequestering in terrestrial ecosystems. *Biogeochemistry* **1**, 219–232.

Vogt, K. A., Grier, C. C., Meier, C. E. and Edmonds, R. L. 1982. Mycorrhizal role in net primary production and nutrient cycling in Abies amabilis ecosystems in Western Washington. *Ecology* **63**, 370–380.

Webb, W. L., Lauenroth, W. K., Szarek, S. R. and Kinerson, R. S. 1983. Primary production and abiotic controls in forests, grasslands, and desert ecosystems in the United States. *Ecology* **64**, 134–151.

Wisniewski, J. and Sampson, R. M. (eds.) 1993. *Terrestrial biospheric carbon fluxes: quantification of sinks and sources of CO_2*. Kluwer Academic, Dordrecht.

Wong, S. C., Cowan, I. R. and Farquhar, G. D. 1979. Stomatal conductance correlates with photosynthetic capacity. *Nature* **282**, 424–426.

Zinke, P. J., Stangenberger, A. G., Post, W. M., Emanuel, W. R. and Olson, J. S. 1986. *Worldwide organic soil carbon and nitrogen data*. NDP-018, Carbon Dioxide Information Center, Oak Ridge National Laboratory, Oak Ridge, Tennessee.